International Journal of Nanomedicine

Dovepress
open access to scientific and medical research

Open Access Full Text Article

ORIGINAL RESEARCH

La_2O_3 Nanoparticles Induce Reproductive Toxicity Mediated by the Nrf-2/ARE Signaling Pathway in Kunming Mice

This article was published in the following Dove Press journal:
International Journal of Nanomedicine

Lu Yuan[1]
Qingzhao Li[1]
Disi Bai[2]
Xueliang Shang[2]
Fen Hu[3]
Zhenfei Chen[4]
Tianyang An[5]
Yajing Chen[6]
Xiujun Zhang[1]

[1]College of Public Health, [2]College of Psychology, [3]College of Life Sciences, [4]Environmental Monitoring Center Tang Shan, Tangshan 063210, Hebei, People's Republic of China; [5]College of Ji Tang, [6]College of Pharmacy of North China University of Science and Technology, Tangshan 063210, Hebei, People's Republic of China

Purpose: Lanthanum oxide (La_2O_3) nanoparticles (NPs) have been widely used in catalytic and photoelectric applications, but the reproductive toxicity is still unclear. This study evaluated the reproductive toxicity of two different-sized La_2O_3 particles in the testes.

Materials and Methods: Fifty Kunming mice were randomly divided into five groups. Mice were treated with La_2O_3 NPs by repeated intragastric administration for 90 days (control, nano-sized with 5, 10, 50 mg/kg BW and micro-sized with 50 mg/kg BW). Mice in the control group were treated with de-ionised water without La_2O_3 NPs. Sperm parameters, testicular histopathology, TEM assessment, hormone assay and nuclear factor erythroid 2-related factor 2 (Nrf-2) pathway were performed and evaluated.

Results: The body weight of mice treated with La_2O_3 NPs or not had no difference; sperm parameters and histological assessment showed that La_2O_3 NPs could induce reproductive toxicity in the testicle. Serum testosterone and gonadotropin-releasing hormone (GnRH) in the NH (nano-sized with 50 mg/kg BW) group were markedly decreased relative to control group, and an increase of luteinizing hormone (LH) in NH group was detected . Additionally, transmission electron microscopy revealed that the ultrastructural abnormalities induced by La_2O_3 NPs were more severe than La_2O_3 MPs in the testes. Furthermore, La_2O_3 NPs treatment inhibited the translocation of nuclear factor erythroid 2-related factor 2 (Nrf-2) from the cytoplasm into the nucleus as well as the expression of downstream genes NAD(P)H quinone oxidoreductase1 (NQO1), hemeoxygenase 1 (HO-1) and (glutathione peroxidase) GSH-Px, thus abrogating Nrf-2-mediated defense mechanisms against oxidative stress.

Conclusions: The results of this study demonstrated that La_2O_3 NPs improved the spermatogenesis defects in mice. La_2O_3 NPs inhibited Nrf-2/ARE signaling pathway that resulted in apoptosis in the mice testes.

Keywords: La_2O_3 nanoparticles, reproductive toxicity, inflammation, Nrf-2/ARE signaling pathway, apoptosis

Correspondence: Xiujun Zhang
North China University of Science and Technology, Bohai Avenue 21, Tangshan 063210, Hebei, People's Republic of China
Tel +86-315-3726335
Fax +86-315-3726341
Email xiujunzhang66@126.com

Disi Bai
College of Psychology, North China University of Science and Technology, Bohai Avenue 21, Tangshan 063000, People's Republic of China
Email baidisi@163.com

Introduction

With the development of engineered nanoparticles (NPs), several NPs such as metal NPs, magnetic NPs, and quantum dots have been widely used in the delivery of drugs, therapeutics, diagnostics, vaccines, and nucleotides. Lanthanum oxide (La_2O_3) NPs are wide-ranging nanomaterials used in sensors, electronics, fuel cells, magnetic data storage, catalysis, and water treatment.[1–6] Due to its widespread use, La_2O_3 NPs are inevitably released in the natural environment, which has adverse effects on the plants and human beings. La_2O_3 NPs can also be combined with other substances in water, and they can be transmitted and get accumulated from low-level to high-level organisms through the food

submit your manuscript | www.dovepress.com
DovePress
http://doi.org/10.2147/IJN.S230949

chain and transmitted to human beings by coming in contact with them in air and soil, by food chain transmission, and by drinking polluted water.[7–13] Lanthanum can accumulate in the brain after its entry via multiple routes, including the skin and the respiratory and gastrointestinal tracts.

Several studies have demonstrated the in vivo toxicity of animal models. Lim et al studied the toxicity of La_2O_3 NPs on Sprague Dawley (SD) rats. Inflammatory effects on BAL decreased over time but lung weight increased and lung proteinosis became severe over time, and the toxicity of La_2O_3 NPs in the lung was more severe than that of La_2O_3 MPs.[14] Male SD rats exposed to La_2O_3 NPs had oxidative stress and inflammation in their lung tissues.[15] Sisler et al found that La_2O_3 NPs produced superoxide radicals that resulted in the stimulation of total tyrosine and threonine phosphorylation in mice, and the release of interleukin-1β (IL-1β) in bronchoalveolar lavage fluid was significantly increased.[16] Li et al found that the change of La_2O_3 NPs' nanostructure from spherical to urchin-like resulted in an increased expression of NLRP3 inflammatory bodies, IL-1β, transforming growth factor-β1, and platelet-derived growth factor-AA. Furthermore, La_2O_3 NPs can induce fibroblast growth factor production, ultimately resulting in pulmonary fibrosis.[17] In an acute oral toxicity study, La_2O_3 NPs could be rapidly absorbed from the gastrointestinal tract and deposited in the liver, resulting in persistent nonspecific hepatotoxicity.[4]

Oxidative stress has generally been considered as an initiating event of reproductive toxicity. In addition, reactive oxygen species can lead to cell injury through several mechanisms, including direct damage to lipid proteins and DNA. Many studies have reported that damage caused by oxidative stress can also decrease endogenous nonenzymatic antioxidants and inhibit antioxidant enzymes. Nuclear factor erythroid 2-related factor (Nrf-2) plays a crucial role in cellular protection against oxidative damage by binding to the antioxidant response element (ARE). ARE is located in the promoter region of genes that encode for Phase II antioxidant enzymes.[18,19] Moreover, testicular injury induced by different-sized La_2O_3 NPs in vivo was insufficiently studied. Thus, this study aimed to investigate the effect of La_2O_3 NPs on testicular toxicity in mice to provide new insights in understanding the mechanism of the biological impacts of La_2O_3 NPs.

Materials and Methods

Characterization of La_2O_3 NPs

La_2O_3 NPs (manufacturer number: Aldrich-634271) used in this experiment were purchased from Sigma-Aldrich (St. Louis, Mo, USA). Micro-sized La_2O_3 (La_2O_3 MPs) was purchased from Maclin Chemical reagent Co., Ltd. (Shanghai, China). These particles were produced under laboratory practices and preserved in the dark until use. The sizes of La_2O_3 NPs were examined using a transmission electron microscope (TF20 Jeol 2100F, USA). The morphology and structure of the nanoparticles were tested by scanning electron microscope (SIGMA HD S4800, USA). The crystalline phase of La_2O_3 NPs was characterized by X-ray diffraction (XRD, Ultima IV, Tokyo, Japan). Scans were performed over the angular range 20−70◦ 2θ at a scan rate of 0.25◦/min at r.t. NPs suspensions were freshly prepared in ultrapure water. Ultrasonic vibration (100 W, 30 kHz) was performed for 30 min before tested. The hydrodynamic diameters were measured using the dynamic light scattering method (Zetasizer Nano ZS 90, Malvern, UK) to check particle size and dispersity.

Establishment of Animal Model

Fifty male Kunming mice (20±2 g) were purchased from the Laboratory Animal Center of North China University of Science and Technology (Animal number SCXK Beijing 2016–0006; Animal center number SYXK Hebei 2005–0038). All animal experiments were approved by the North China University of Science and Technology Institutional Animal Care and Use Committees (2019–053), and all experiments were performed following the Institutional Animal Care and Use Committee of National Tissue Engineering Center (Shanghai, China) guidelines and regulations.

The mice were housed in plastic cages in a controlled environment of 22°C–26°C, with 55%–60% humidity and a 12 h light/dark cycle. For dose selection, we consulted the Organisation for Economic Co-operation and Development (OECD) of 401. According to that report, the LD50 of orally administered La_2O_3 NPs in rats is >12 g/kg BW. These doses were approximately equal to 0.15–0.7 g La_2O_3 NPs exposure in humans with 60–70 kg body weight, which is considered a relatively safe dose range. Mice were divided into 5 groups (control, nano-sized with 5, 10, 50 mg/kg BW and micro-sized with 50 mg/kg BW), which were termed the CON, NL, NM, NH and WM groups; mice were treated with La_2O_3 NPs by repeated intragastric administration for 90 days. Mice in the control group were treated with de-ionised water without La_2O_3 NPs, which was prepared according to the same process by which the La_2O_3 NPs suspension was prepared. The nanoparticles were freshly prepared every day based on the body weights of the mice and were used immediately. The suspension was subjected to ultrasonic vibration (100 W, 30 kHz) for

30 min before intragastric administration. Animals were sacrificed after the last exposure. Testes were immediately isolated and weighed.

ICP-MS Analysis of La

All tissues and organs were removed from −80°C. A 0.1 g of the tissues was digested with HNO_3 by the microwave digestion system. Then, the digested solution was heated at 180°C to remove the residual HNO_3 until it was colorless and clear. The remaining solution was adjusted to 10 mL with 2% HNO_3 solution and the content of La was determined by the ICP-MS. The ICP-MS working conditions were auxiliary gas flow, 1.08 L/min; atomization pressure, 32Ibf/in2; frequency, 27.12; emission power, 1420 w; injection speed, 1.85 mL/min; dilute nitric acid (2%) flushing time, 1 min; ultrapure water flushing time, 1 min. The final contents reported were normalized based on the tissue weight. The same process without tissues was performed to prepare the blank samples.

Histological Assessment

The fixed testis samples were embedded in paraffin, 6 μm thick testes histological sections were cut and stained with hematoxylin-eosin to detect morphological alterations by a light microscope (Olympus IX71, Japan).

Testicular Tissues Ultrastructure Observation

The testes tissues were excised and immediately fixed in 2.5% glutaraldehyde overnight. Then, the samples were rinsed three times with 0.1 M PBS and postfixed with 1% osmic acid for 2 h. After being rinsed three times with 0.1 M PB and serially dehydrated with 50%, 70%, 80%, 90%, and 100% alcohol and 100% acetone, the samples were embedded in epoxy resin. The ultrathin sections (70 nm) were obtained by an ultramicrotome (TF20 Jeol 2100F, USA). Then, the sections were stained with lead citrate and uranyl acetate for 5–10 min and observed by TEM. The pathologist was blinded to identity and analysis of the ultrathin sections.

Effects of La_2O_3 NPs and MPs on Sperm Parameters

The sperm motility (%), sperm count (million/mL), and the rates of sperm survival (%) were investigated in this study. The testis and epididymis were collected after mice were sacrificed, and immediately placed in the centrifuge tube with 37 °C preheated physiological saline and cut up, put into 37 °C water-bath, then incubated for 20 min; sperm motility was detected visually at a light microscope at 37 °C (400×). Semen were collected, pretreated at 60 °C for 10 min, added as a suspension to the hemocytometer, and sperm count observed with light microscope (200×). One drop of sperm suspension was placed on a prewarmed glass slide for light microscopic observation of sperm motility. A total of 200 sperms per sample were evaluated. The percentage of sperms with forward and progressive activity was counted to assess sperm motility.

Measurement of Testosterone, LH, Follicle Stimulating Hormone (FSH) and GnRH Levels

The serum testosterone, LH, FSH and GnRH levels were measured with commercially available immunoassay kits purchased from Shanghai Enzyme-linked Biotechnology for testosterone (ml001948, China) and Nanjing MR Ng Biotechnology for LH, SBJ-M0408; FSH, SBJ-M0479 and GnRH, SBJ-M0558). Manufacturer instructions were followed to perform these assays. All assays were performed in triplicates, and the mean concentration was calculated.

Measurement of MDA Levels, SOD and CAT Activities

After intragastric administration of La_2O_3 NPs and MPs, the levels of MDA and activities of SOD and CAT in the testis were tested using the following assay kits: A001-1-2, A003-3-1 and A007-2-1 (Nanjing Jiancheng Bioengineering Institute, China). The steps were based on the manufacturers' protocol. All assays were performed in triplicate.

Immunohistochemistry

Formalin-fixed paraffin-embedded testicular tissue sections of all groups were deparaffinised and soaked in graded concentrations of ethanol. The procedures were performed following the manufactures' instructions. After dewaxed, sections were incubated in solution containing rabbit BAX and NF-κB polyclonal antibodies (1: 200, Bioss Biotechnology, Inc., Beijing, China) for 3 h at 37° C. Next, biotin-labelled anti-rabbit secondary antibody (Boster Bioengineering Co., Ltd., Wuhan, China) was added, and the sections were incubated for 30 min at room temperature. Thereafter, reactions were visualized with 3, 3′-diaminobenzidine-tetrahydrochloride (DAB) and counterstained in haematoxylin.

Transferase dUTP Nick End Labelling (TUNEL) Assay

Testis tissues processed for the analysis of apoptosis-related DNA strand breaks were also analyzed using an In situ Cell Death Detection kit, POD (Roche Diagnostics, Shanghai, China). The steps of incubation and staining were based on the manufacturer's introduction, and the following procedures were performed.[20] Afterwards, the percentage of seminiferous tubules containing TUNEL-positive germ cells and the TUNEL-positive germ cells per seminiferous tubule were calculated.

Quantitative Real-Time PCR

Total RNA of the testis samples was extracted using an RNeasy mini kit (Qiagen, Tokyo, Japan) according to the manufacturer's protocol. The cDNA was synthesized from total RNA 5 mg using murine leukemia virus reverse transcriptase and Oligo-dT primers (BGI, Beijing, China). Quantitative real-time RT-PCR was used to quantify the expression levels of different genes, using β-actin mRNA as the normalization standard. The probes for genes, including StAR, CYP11A1, CYP17A1, LHR, Keap-1, Nrf-2, NQO1, HO-1, GSH-Px, iNOS, IL-1β, TNF-α, COX-2, Bcl-2 and BAX were designed by the manufacturer and purchased from were designed and synthesized by Beijing Genomics Institute (BGI). Sequences of the forward and reverse primers are listed in Table 1. Amplification was performed under the following conditions: 1 min at 95 °C; 5 s at 95 °C; 30 s at 60 °C with for 40 cycles, Melt Curve 65°C to 95°C. qRTPCR of mRNAs was performed using Platinum SYBR Green qPCR Super Mix UDG Kit (Invitrogen), and real-time PCR experiments were carried on the Thermo system (7900HT). Gene expression levels were calculated as a ratio to the expression of the reference gene, and data were analyzed using the $2^{-\Delta\Delta Ct}$ method.

Western Blotting Analysis

The expression of StAR, CYP11A1, CYP17A1, LHR, Keap-1, Nrf-2, NQO1, HO-1, GSH-Px, COX-2, iNOS, IL-1β, TNF-α, Bcl-2 and BAX was assayed by Western blotting. Frozen tissue samples were homogenized and lysed in RIPA (Sangon Biotech, Shanghai, China) for 20 min, and centrifuged 13.000×g for 15 min at 4 °C, and supernatants were collected. BCA protein assay kit was used to determine the total protein concentrations (Sangon Biotech, Shanghai, China). A 40μg total protein was loaded onto 8% sodium dodecyl sulfate (SDS) polyacrylamide gel, separated, and transferred to a 0.45 μm PVDF membrane (Pall, Gelman Laboratory, USA); then, membranes were blocked with 5% BSA in buffer for 2 h at room temperature. Followed by incubation with antibodies against specific primary antibodies: anti-StAR (12225-1-AP, diluted at 1:1500, Proteintech, USA), anti-CYP11A1 (13363-1-AP, diluted at 1:2000, Proteintech, USA), anti-CYP17A1 (ab125022, diluted at 1:1000, Abcam, Cambridge, UK), anti-LHR (19968-1-AP, diluted at 1:500, Proteintech, USA), anti-Keap-1 (60027-1-Ig, diluted at 1:500, Proteintech, USA), anti-Nrf-2 (16396-1-AP, diluted at 1:5000, Proteintech, USA), anti-NQO1 (ab80588, diluted at 1:1000, Abcam, Cambridge, UK), anti-HO-1 (27282-1-AP, diluted at 1:1500, Proteintech, USA), anti-GSH-Px (sc-166120, diluted at 1:500, Santa Crus, USA), anti-TNF-α (17,590-1-AP, diluted at 1:1000; Proteintech, USA), anti-IL-1β (16806-1-AP, diluted at 1:300, Proteintech, USA), anti-i-NOS (18985-1-AP, diluted at 1:600, Proteintech, USA), anti-COX-2 (BA0738, diluted at 1:400, BOSTER, China), anti-BAX (diluted at 1:1000, Abcam, Cambridge, UK), anti-Bcl-2 (diluted at 1:1000, Abcam, Cambridge, UK), and rabbit diluted 1:10,000; anti-β-actin (ARH4149, Antibody Revolution, USA) overnight at 4°C, washed 3 times in TBST for 10 min, and incubated with horseradish peroxidase-conjugated goat anti-rabbit IgG or goat anti-mouse IgG antibody (1:1000; Abgent, San Diego, CA, USA) for 1 h. Densitometric analysis was normalised using β-actin as an internal control. Bands were visualised using an enhanced chemiluminescence (ECL) kit (Sangon Biotech). Quantity One software was used to quantify each band area and density on the blots. Quantified band intensities are presented as the fold-change from the control. The experiments were repeated three times and were performed independently.

Statistical Analysis

All differentiation experiments were done using at least three independent groups. Data are shown as the mean ± SD. Group comparisons were made using one-way ANOVA followed by post hoc Tukey's test. A P-value<0.05 was considered statistically significant.

Table 1 List of Primers Used for Real-Time RT-PCR

Function	Gene Name	Primer Sequence (5′-3′)	Product (bp)	Genbank Accession
Testosterone synthesis-related genes	*StAR*	F: CGGGTGGATGGGTCAAGTTC R: GCACTTCGTCCCCGTTCTC	188	NM_011485.5
	CYP11A1	F: AGGTCCTTCAATGAGATCCCTT R: TCCCTGTAAATGGGGCCATAC	137	NM_019779.4
	CYP17A1	F: AGTCAAAGACACCTAATGCCAAG R: ACGTCTGGGGAGAAACGGT	83	NM_007809.3
	LHR	F: CTCGCCCGACTATCTCTCAC R: ACGACCTCATTAAGTCCCCTG	77	NM_013582.3
Nrf-2/ARE pathway-related genes	*Keap-1*	F: CGGGGACGCAGTGATGTATG R: TGTGTAGCTGAAGGTTCGGTTA	85	NM_016679.4
	Nrf-2	F: TAGATGACCATGAGTCGCTTGC R: GCCAAACTTGCTCCATGTCC	153	NM_010902.4
	NQO1	F: AGGATGGGAGGTACTCGAATC R: TGCTAGAGATGACTCGGAAGG	127	NM_008706.5
	HO-1	F: AGGTACACATCCAAGCCGAGA R: CATCACCAGCTTAAAGCCTTCT	86	NM_010442.2
	GSH-Px	F: GAAGTGCGAAGTGAATGG R: TGTCGATGGTACGAAAGC	224	NM_008160.6
Inflammation	*iNOS*	F: GTTCTCAGCCCAACAATACAAGA R: GTGGACGGGTCGATGTCAC	127	NM_010927.4
	IL-1β	F: GAAATGCCACCTTTTGACAGTG R: TGGATGCTCTCATCAGGACAG	116	NM_008361.4
	TNF-α	F: CATGGATCTCAAAGACAACCAA R: CTCCTGGTATGAAATGGCAAAT	193	NM_013693.3
	COX-2	F: TACAACAACTCCATCCTCCTTG R: TTCATCTCTCTGCTCTGGTCAA	186	NM_011198.4
Apoptosis	*Bcl-2*	F: GGTCTTCAGAGACAGCCAGG R: GATCCAGGATAACGGAGGCT	113	NM_177410.3
	BAX	F: GATCAGCTCGGGCACTTTAG R: TTGCTGATGGCAACTTCAAC	120	NM_007527.3
Reference	*β-actin*	F: GTGCTATGTTGCTCTAGACTTCG R: ATGCCACAGGATTCCATACC	174	NM_007393.5

Results

Characterization of La_2O_3 NPs

The size and surface morphology of both La_2O_3 NPs and MPs were examined using SEM. The SEM images are given in Figure 1A, and showed that the La_2O_3 NPs and MPs are irregular sheet structure. The sizes of La_2O_3 NPs were uniform in size in the region of 500 nm as seen in Figure 1Aa. From Figure 1Ab it was clear that these MPs were almost flake in shape about 1000 nm. The TEM images of La_2O_3 NPs and MPs are given in Figure 1B, and the size of most NPs was about 500 nm, showing aciniform aggregates and agglomerates in Figure 1Ba, and the agglomerates of La_2O_3 MPs (Figure 1Bb) were about 1000nm. The average sizes were calculated in the column chart (Figure 1Bc). TEM revealed La_2O_3 NPs aggregates, black dots, in adipose and connective tissues in the scrotum of mice exposed to La_2O_3 NPs for 90 days (Figure 1Bd), but not aggregates in La_2O_3 MPs treated group (Figure 1Be). It can be observed in XRD spectrum that there are sharp characteristic diffraction peaks and no other impurity peaks, which indicated that La_2O_3 NPs and MPs had high purity and crystallinity (Figure 1C). Hydrodynamic diameter and zeta-potential in DI water, PBS or at pH 2.98, 4.04 and 4.74 were measured. A solution is considered stable if the zeta potential value is more

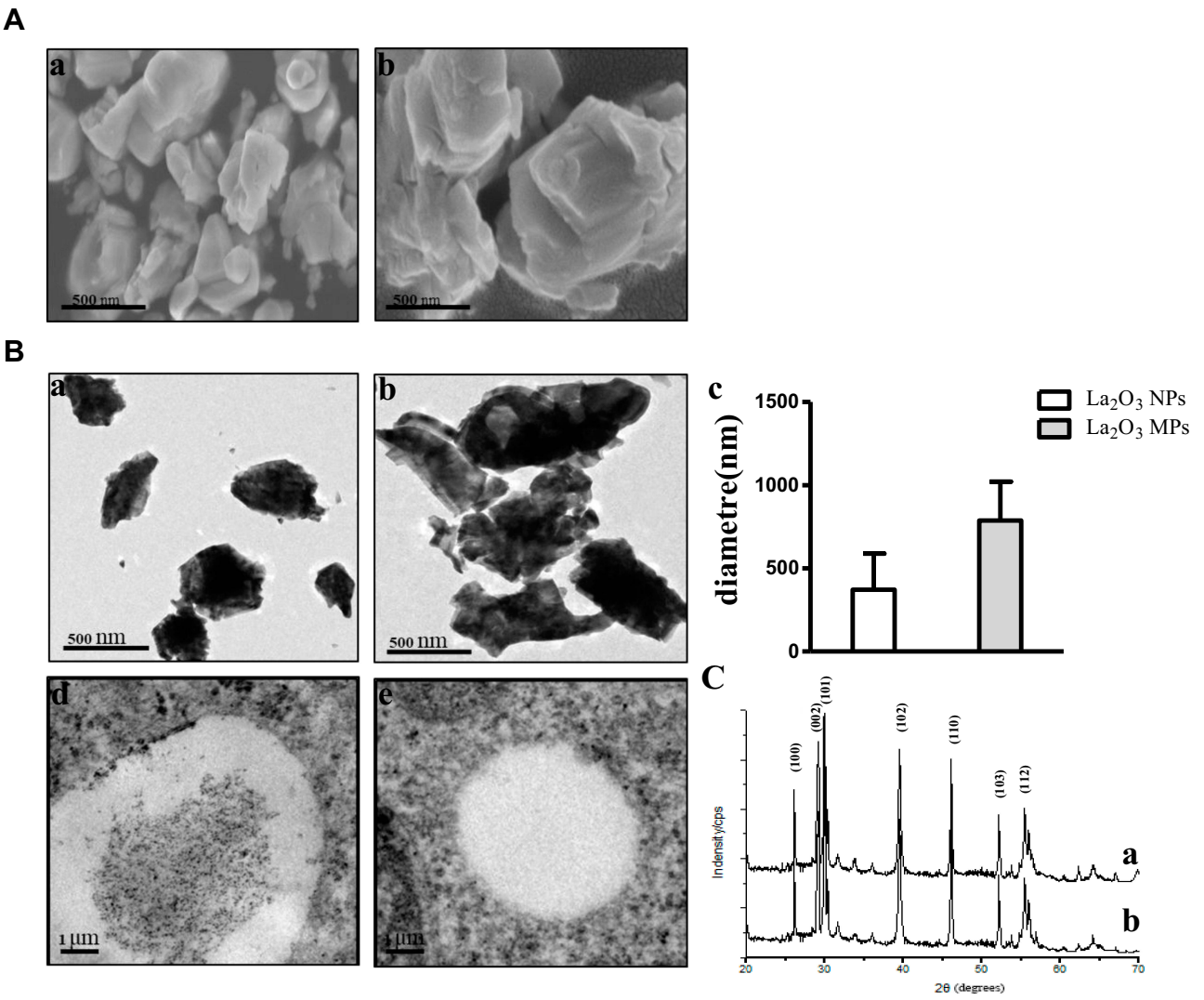

Figure 1 The characterization of the La_2O_3 NPs and La_2O_3 MPs. (**A**) The SEM images of La_2O_3 NPs (a) and La_2O_3 MPs (b) at high magnification, and the particles were in irregular sheet structure. Scale bar = 500 nm. (**B**) The TEM images of La_2O_3 NPs (a) and La_2O_3 MPs (b) at high magnification, showing aciniform aggregates and agglomerates in Figure 1Ba, and the average sizes of La_2O_3 NPs and La_2O_3 MPs in (c). (d) and (e): La_2O_3 NPs and La_2O_3 MPs bioaccumulate in scrotal tissues by TEM analysis. Scale bar = 1 μm. (**C**) The XRD patterns of the La_2O_3 NPs (a) and La_2O_3 MPs (b).

negative than −30mV or more positive than +30mV.[20] The results showed the agglomeration of the La_2O_3 NPs with the PH decreased, and the LDV results showed the La_2O_3 NPs had zeta potential value higher than 30mV in the mentioned solutions (Table 2).

Mice Growth, Coefficients and Testicular Histology

In our present study, no deaths or abnormal clinical signs were observed in any of the group. The body weights of mice in the 5 groups were compared, and the differences were not statistically significant (Figure 2A, $P>0.05$). Mice in the control and La_2O_3 MPs groups had normal testicular architecture and germinal cell arrangement. NM and NH groups showed vacuolation with disorganized germinal

Table 2 Characteristics of La_2O_3 NPs in the Different pH Values Solutions

Particle	PH	Average Diametre (nm)	PdI	Zeta Potential (mV)
La_2O_3 NPs	2.98	739.72	0.432	32.72
	4.04	462.38	0.375	33.21
	4.74	361.83	0.276	38.86
	In DI water	284.32	0.462	32.17
	In PBS	395.71	0.489	36.65

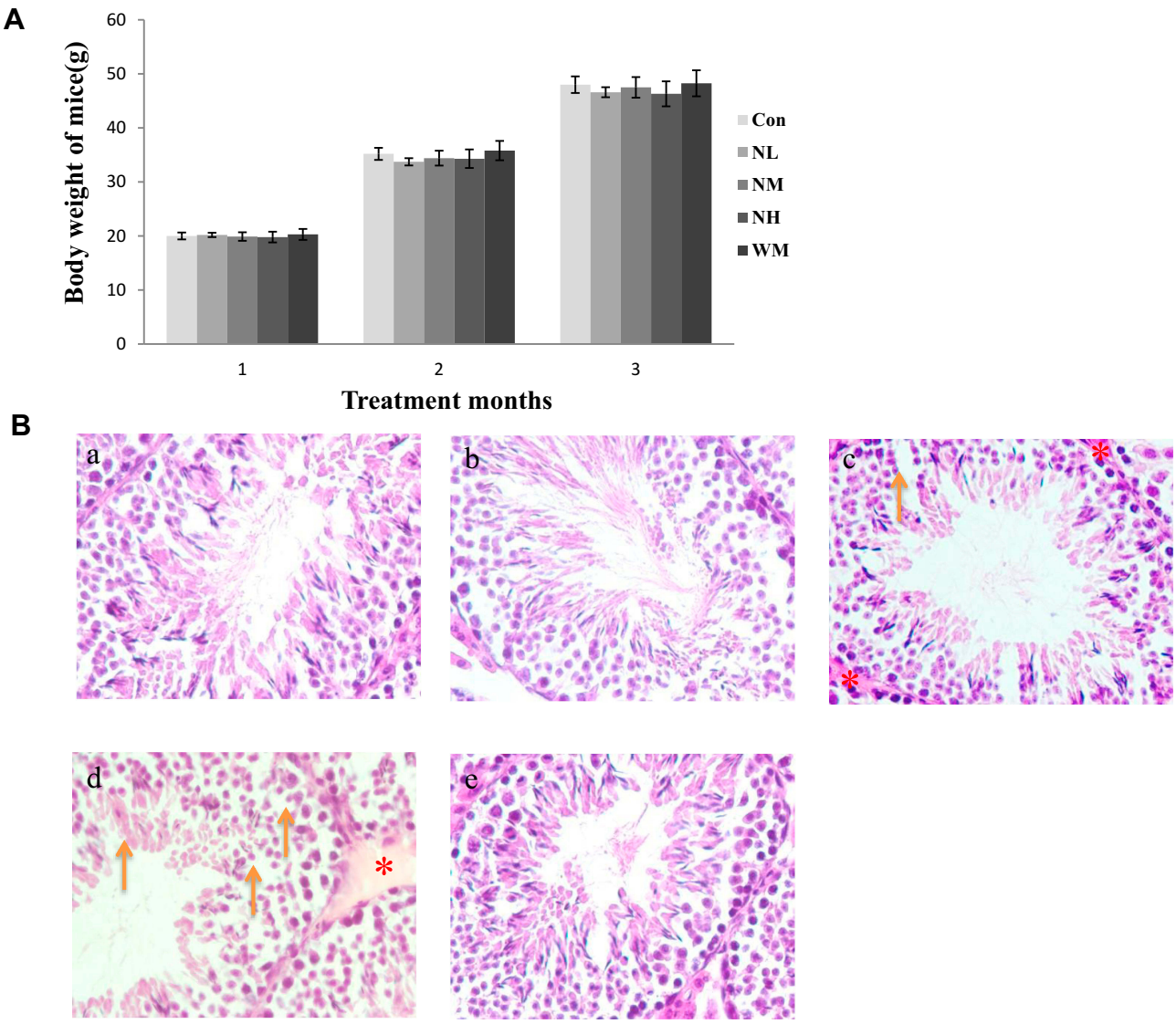

Figure 2 Effects of La_2O_3 NPs on mouse growth and testicular histology. (**A**) The body weights of mice in the 5 groups were compared, and the differences were not statistically significant (Figure 2A) ($P > 0.05$). (**B**) Histopathological changes in murine testes caused by intragastric administration of La_2O_3 NPs for 90 days. The testes from control (a), NL (b) and WM (e) groups showed normal morphology and spermatogenesis. In the NM and NH (c and d) groups, the testes exhibited vacuole-like changes in the spermatogenic epithelium, as indicated by arrows (×400). Moreover, moderate LCs edema (asterisk) were observed in NM and NH groups.

epithelium and disorganization of germ cell layers including sloughing, detachment and vacuolization are markedly increased (Figure 2B). Effects of La_2O_3 NPs and MPs on coefficients of mice are shown in Table 3. These observations showed that La_2O_3 NPs exposure had induced apoptosis in the germ cells in the testes.

The La Contents in Tissues and Whole Blood

After intragastric administration of La_2O_3 NPs (5, 10 and 50 mg/kg BW) and La_2O_3 MPs (50 mg/kg BW) for 90 days, organs of brain, heart, testis, spleen, kidney, liver and whole blood were measured for La contents. As shown in Table 4, compared with the control and WM groups, the La contents in the testicles of mice in the NM and NH groups were significantly higher than in mice in the control group ($P<0.01$). These results suggest that La_2O_3 NPs can be absorbed and distributed to tissues through the circulatory system and can be deposited in the brain, heart, testis, spleen, kidney and liver.

Effects of La_2O_3 NPs and MPs on Testicular Ultrastructure

The ultrastructure of testes following exposure to La_2O_3 NPs was examined by TEM. In the control group no morphological changes were found (Figure 3A). Similar

Table 3 Effects of Different Doses of La_2O_3 NPs and MPs on Coefficients of Mice

	Coefficients of Tissues				
Tissue	**Con**	**NL**	**NM**	**NH**	**WM**
Liver (mg/g)	49.47 ±2.24	49.95 ±2.61	51.21 ±1.82	55.49 ±2.43*	52.42 ±2.67
Kidney (mg/g)	15.19 ±0.79	14.74 ±0.56	15.01 ±0.84	15.94 ±0.92	15.15 ±0.74
Lung (mg/g)	5.57 ±0.69	5.36 ±0.68	5.75 ±0.47	5.78 ±0.31	5.45 ±0.97
Spleen (mg/g)	2.89 ±0.36	2.96 ±0.23	3.52 ±0.38	3.81 ±0.42*	3.33 ±0.27
Heart (mg/g)	5.19 ±0.33	5.14 ±0.41	5.07 ±0.65	5.01 ±0.78	5.22 ±0.60
Brain (mg/g)	17.89 ±0.86	17.32 ±1.54	16.07 ±0.87	16.89 ±0.72	16.35 ±1.02
Testis (mg/g)	2.87 ±0.35	3.03 ±0.77	2.86 ±0.23	2.84 ±0.18	2.76 ±0.43

Notes: Values are expressed as mean ± SD for 10 mice per group *Significantly different from vehicle control at $P<0.05$.

to the controls, NL (Figure 3B) and WM (Figure 3E) groups revealed a normal fine structure and slightly affected. As the doses of La_2O_3 NPs increased, vacuolation of the mitochondria was detected in affected tubules. Moreover, in affected tubules, vacuolation was detected in the seminiferous epithelium in the NM and NH groups (Figure 3C–D). These results demonstrate that La_2O_3 NPs may change the testicular ultrastructure and cause reproduce toxicity.

Table 4 The La Contents in Whole Blood and Different Organs

	Con	**La_2O_3 NPs**			**La_2O_3 MPs**
		NL	**NM**	**NH**	**WM**
Liver (μg/g)	5.32 ±0.75	82.21 ±4.35**	148.38 ±18.47**	434.98 ±71.12**	84.75 ±14.25**Δ
Kidney (μg/g)	3.53 ±0.58	56.17 ±7.26**	94.52 ±15.72**	366.52 ±48.53**	67.31 ±7.49**Δ
Spleen (μg/g)	2.85 ±0.31	48.92 ±7.81**	82.32 ±13.31**	343.35 ±37.57**	54.68 ±8.42**Δ
Testis (μg/g)	3.37 ±0.54	43.58 ±6.26**	75.62 ±15.17**	276.72 ±34.45**	45.16 ±11.27**Δ
Lung (μg/g)	4.15 ±0.62	35.53 ±6.23**	67.25 ±18.54**	214.16 ±37.31**	27.55 ±8.58**Δ
Brain (μg/g)	3.28 ±0.38	31.47 ±4.32**	51.51 ±7.86**	102.87 ±27.62**	24.68 ±9.40**Δ
Heart (μg/g)	3.62 ±0.37	9.81 ±0.89*	21.56 ±7.34**	63.45 ±12.37**	8.31 ±0.45Δ
Blood (μg/mL)	4.28 ±0.75	84.65 ±9.52**	156.30 ±15.97**	468.36 ±58.72**	86.68 ±8.82**Δ

Notes: Values are expressed as mean ± SD for 5 mice per group. *,**Significantly different from vehicle control at $P < 0.05$ and $P < 0.01$; ΔSignificantly different from NH vs WM group at $P<0.05$.

The Effect of La_2O_3 NPs and MPs on Sperm Parameters and Levels of Testis Testosterone

As shown in Figure 4A, after intragastric administration of La_2O_3 NPs and MPs the percentage of sperm count in the NM and NH groups were decreased ($P<0.05$), and the sperm motility and sperm survival percentages in NH group were significantly decreased ($P<0.05$), but no statistical significance was attained in the NL and WM groups compared to the controls ($P>0.05$). Because the levels of testis testosterone were regulated in part by levels of GnRH, LH and FSH. These levels were involved in the synthesis and regulation of testosterone in the testes. Serum testosterone and GnRH in the NH group were decreased dramatically by 33.2% and 29.32% ($P<0.05$) relative to control groups. To detect changes in the hypothalamic-pituitary-gonadal (HPG) axis, an elevated serum LH was found, up to 28.7% compared to control ($P<0.05$). An increase of LH in NH group was due to the decreased inhibitory activity of serum testosterone on the HPG axis via the negative feedback mechanism (Figure 4B). However, no significant differences were found in the levels of testis FSH among the groups ($P>0.05$).

The Effect of La_2O_3 NPs and MPs on Genes and Proteins Involved in Synthesis of Testosterone

As shown in Figure 4C, the testis testosterone level was also regulated by the genes and proteins involved in the synthesis of testosterone from bound cholesterol in the bloodstream, including StAR, CYP11A1, CYP17A1, and LHR. qRT-PCR results showed that LHR mRNA expression levels increased significantly in the NH groups (1.47-fold) relative to the control group, StAR, CYP11A1 and CYP17A1 mRNA expression levels decreased significantly to 0.36-fold, 0.53-fold and 0.49-fold, respectively. Furthermore, LHR protein expression levels by Western blotting confirmed the increasing mRNA expression in the LHR gene in the NH group (Figure 4D, $P<0.05$).Protein expression levels of StAR, CYP11A1 and CYP17A1 were confirmed by Western

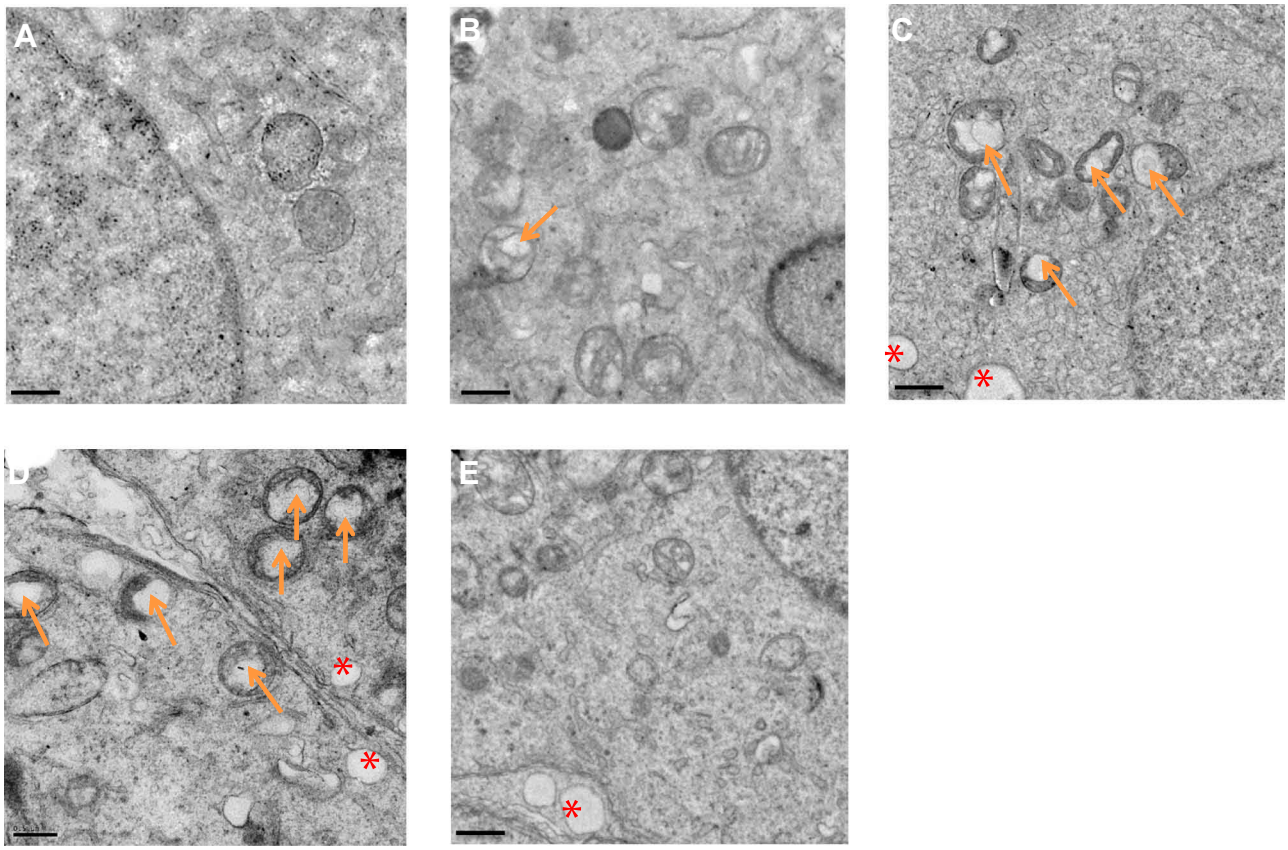

Figure 3 La_2O_3 NPs and MPs influence on ultrastructure of testis. (**A**) Control. (**B**) La_2O_3 NPs (5 mg/kg). (**C**) La_2O_3 NPs (10 mg/kg). Arrows indicate mitochondria and vacuoles in mitochondria. (**D**) La_2O_3 NPs (50 mg/kg). (**E**) La_2O_3 MPs (50 mg/kg) (×8000). The control and La_2O_3 MPs groups showed no morphological changes, but vacuolar changes in the mitochondria were detected in the NM and NH groups (arrows). In affected tubules, vacuolation of the seminiferous epithelium could be detected (red asterisk).

blotting of mRNA expression in the NH group (Figure 4D).

Oxidative Stress Analysis

The oxidative stress levels of MDA and activities of SOD and CAT were detected. SOD activities in NH group were significantly reduced compared to the control group (Figure 5Aa). In addition, the NM and NH groups of MDA levels were markedly increased ($P<0.05$), while the levels in the NL and WM groups were almost equivalent to that of the control group (Figure 5Ab). As CAT activity was an indicator of oxidative damage to testes, a significant decrease in CAT activity was detected in the NH group (Figure 5Ac). The results showed that high doses of La_2O_3 NPs-induced oxidative stress in the testis of exposed mice.

Effects of La_2O_3 NPs and MPs on Nrf-2/ARE Pathway

The expression of Nrf-2/ARE pathway-related genes and protein expressions of qRT-PCR results showed that Nrf-2, NQO1, HO-1 and GSH-Px mRNA expression levels decreased significantly to 0.39-fold, 0.53-fold, 0.44-fold and 0.58-fold, respectively, whereas the expression level of Keap-1 increased to1.39-fold in NH group (Figure 5B, $P<0.05$). Furthermore, the Nrf-2/ARE pathway related protein expression levels by Western blotting to confirm the mRNA expressions. As shown in Figure 5C, the protein levels of Nrf-2, HO-1, NQO1 and GSH-Px in the NH groups were decreased significantly ($P<0.05$). These results evidenced that the inhibition of the Nrf-2/ARE signaling pathway is induced by La_2O_3 NPs exposure.

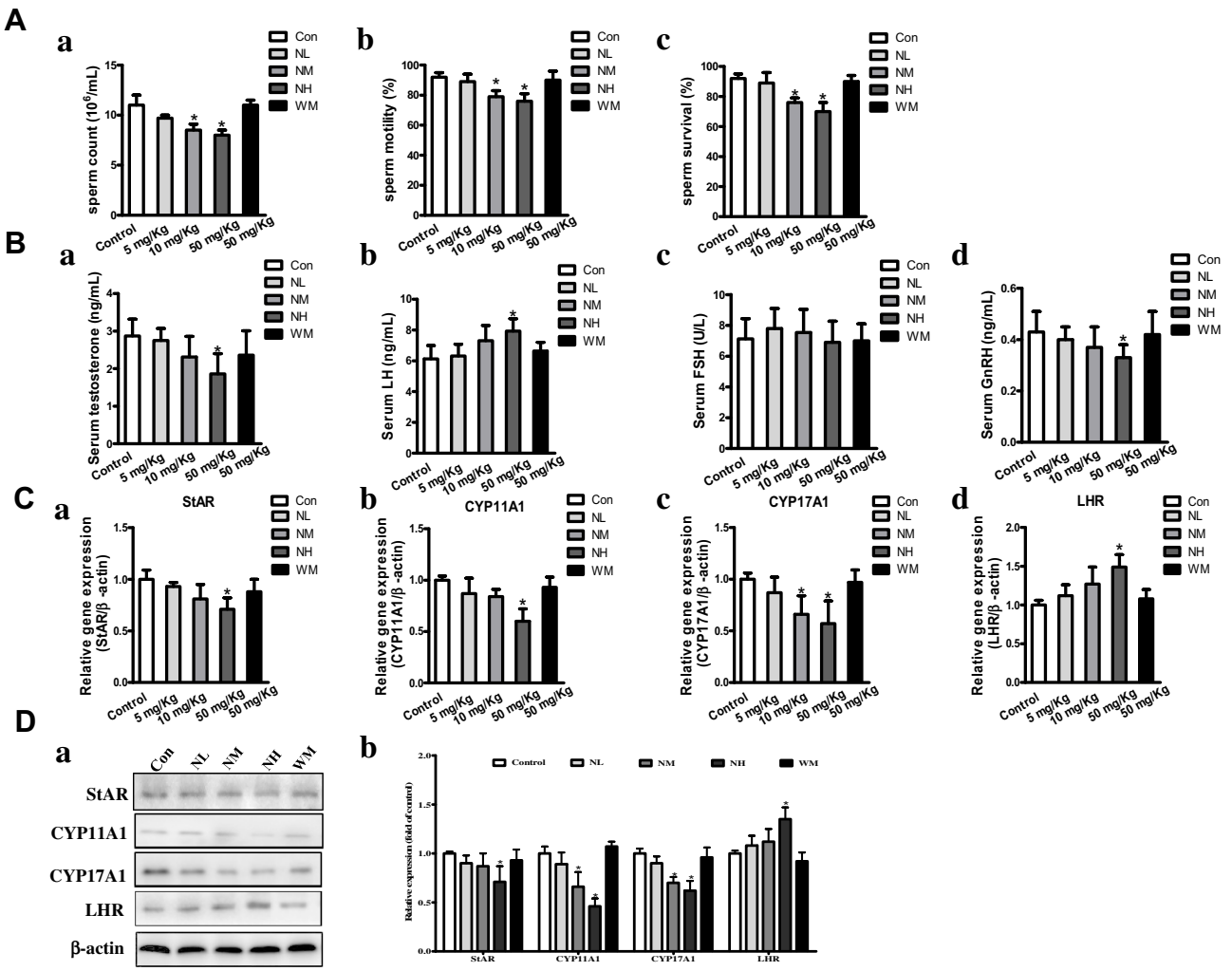

Figure 4 The impact of La_2O_3 NPs and MPs on sperm parameters, levels of testis testosterone, genes and proteins involved in synthesis of testosterone. Changes in sperm count (**A**a) and sperm motility percentages (**A**b) and sperm survival percentages (**A**c) of the mice; (**B**a) testis testosterone; (**B**b) LH levels; (**B**c) FSH levels; (**B**d) GnRH levels in the 90 days intragastric exposures. (N=10, mean S.D.). *P <0.05 vs control group. Effects of La_2O_3 NPs and MPs on mRNA expression of StAR, CYP11A1, CYP17A1 and LHR in testes (**C**a-d). Effects of La_2O_3 NPs and MPs on protein expression of StAR, CYP11A1, CYP17A1 and LHR (**D**a-b). β-Actin was used as the internal control. *P<0.05 vs control.

Effects of La_2O_3 NPs and MPs on Testicular Inflammation

Compared with the control group, the number of NF-κB-positive cells was significantly increased in the NM and NH groups (P<0.05). However, in the NL and WM groups, no significant differences were found compared with the control group (Figure 6A, P>0.05). In the NM and NH groups, the iNOS, IL-1β, TNF-α and COX-2 were elevated in the NM and NH groups (P<0.05) (Figure 6B). Furthermore, the expression levels of iNOS, IL-1β, TNF-α and COX-2 were validated by Western blotting analysis, as shown in Figure 6C. The expression levels of iNOS, IL-1β, TNF-α and COX-2 in the NH group were increased by, 1.62-, 1.68-, 1.72- and 1.57-fold, respectively (P<0.05). The results elucidated La_2O_3 NPs could induce testicular inflammation.

Effects of La_2O_3 NPs and MPs on Germ Cells Apoptosis

TUNEL assay was performed to identify the apoptotic cells in seminiferous tubules (Figure 7A). In the control group, few TUNEL-positive cells could be found, which indicates a basal level of germ cell apoptosis. However, the number of TUNEL-positive cells was lower in the NL and WM groups than in the NH group (P<0.05). Compared with the control group, TUNEL-positive cells were increased in the NH group (P<0.05). Compared with the control group, the BAX-positive cells were significantly increased in the NM

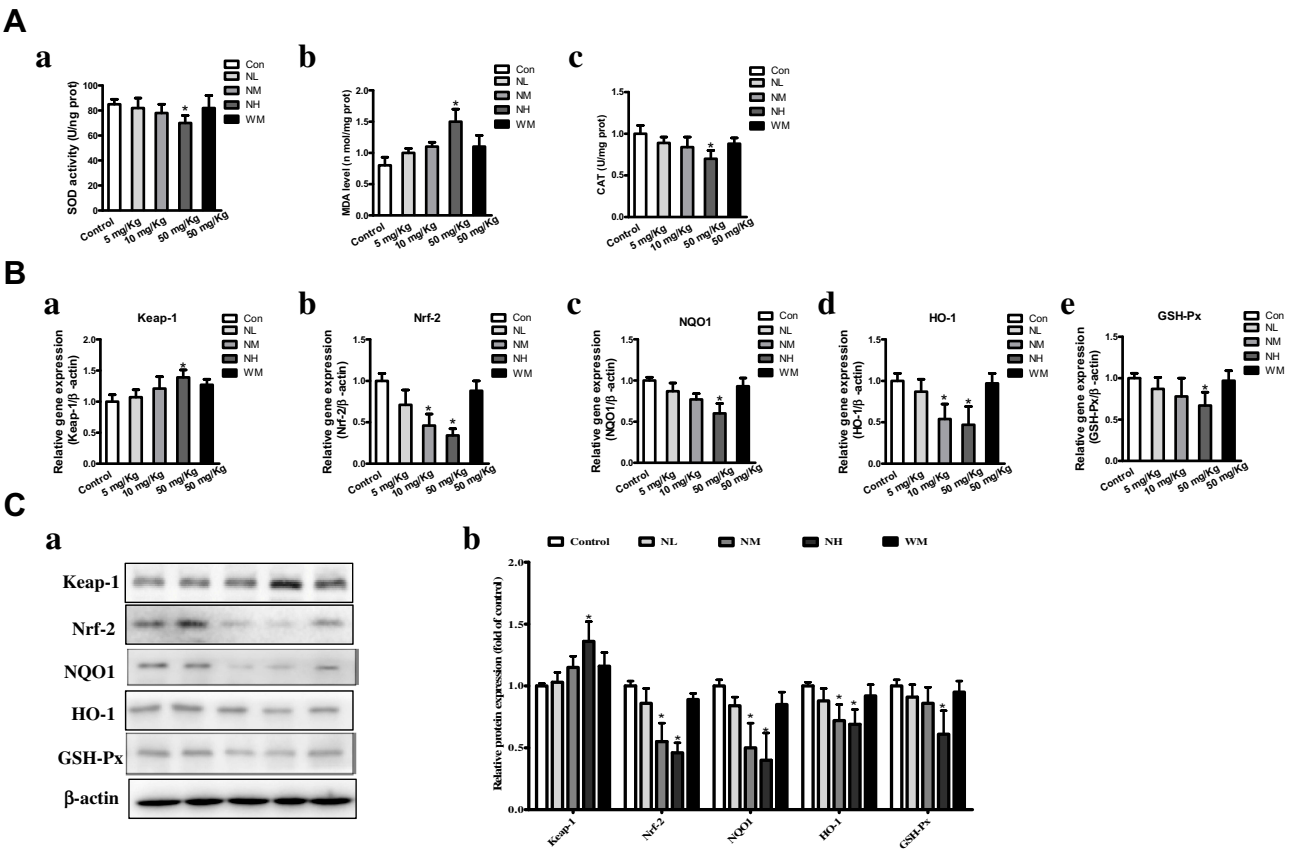

Figure 5 La_2O_3 NPs and MPs induced Nrf-2/ARE signaling changes in mice testes. (**A**) Effects of La_2O_3 NPs and MPs on MDA level, SOD and CAT activities. (a) SOD level. (b) MDA activity. (c) CAT activity. (**B**) La_2O_3 NPs and MPs infleuenced on Nrf-2/ARE signaling relative genes in mouse testes. Effects on mRNA expression levels of Keap-1, Nrf-2, NQO1, HO-1 and GSH-Px in mice testes. (Ca-Cb) The protein levels of Nrf-2/ARE signaling relative genes by western blotting.

and NH group (Figure 7B, $P<0.05$). Bcl-2 was down-regulated in NH group, and BAX was up-regulated both in the gene and protein levels in NH groups (Figure 7C–D, $P<0.05$). These investigations revealed that the apoptosis and changes in the expression of related genes in the testes of mice exposed to La_2O_3 NPs.

Discussion

The increasing application of nanoscience and nanotechnologies to consumer products has raised concerns about their potential risks to human health. The male reproductive system is known to be more sensitive to exogenous materials than other organ systems and has been susceptible to damage by harmful substances in recent years.[21] Previous studies demonstrated that NPs could induce testicular damages in a dose-dependent manner in mice, and the lesions were considered early morphological signs of testicular injury with the main Sertoli cell (SC) response to several xenobiotics.[22] It is essential to identify the testis toxicity of La_2O_3 NPs, and the difference in toxicity between La_2O_3 NPs and La_2O_3 MPs in mice testis has not been investigated. Yang et al found that large-sized particles exhibited less active in exerting toxicological or biological responses than the small-sized particles.[23] While Grassian et al found that the smaller particles did not cause a larger inflammatory response than the larger particles, larger NPs were found to be more toxic than smaller NPs.[24] Lu et al found that not only nano-sized but also submicro-sized silica particles could cause a similar extent of liver injury, which is dependent on the exposure dose, and the mechanism of toxicity may almost be similar.[25] Overall, the association between particle size and tissue damage by nanomaterials is unclear and the evidence is contradictory. Therefore, it is necessary to investigate the association between toxicity and particle size of La_2O_3 NPs. The current work hypothesised that La_2O_3 nanoparticles primarily inhibit the Nrf-2/ARE signalling cascade, subsequently inducing apoptosis. This results in a reduction in sperm concentration and pathological impairment in the seminiferous tubules of

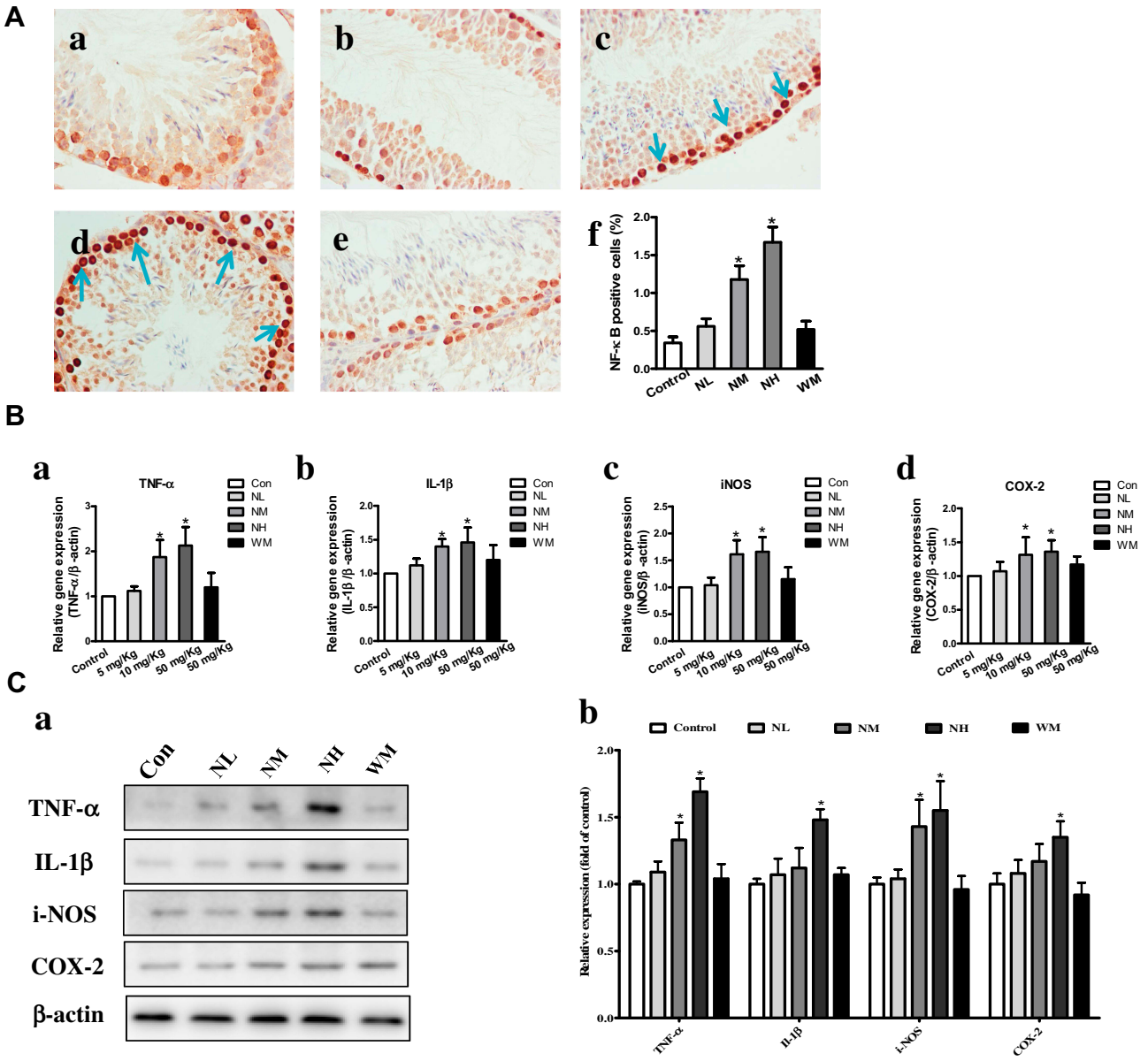

Figure 6 Effects of La_2O_3 NPs and MPs on testicular inflammation. (**A**) Inflammation testicular cells in the control group (a), NL group (b), NM group (c), NH group (d) and WM group (e). NF-κB-positive cells (f) were significantly increased in the NM and NH groups (×400, $P<0.05$). However, in the NL and WM groups no significant differences were found compared with control group (Figure 6A, $P>0.05$). The expressions of expression levels of inflammatory enzymes iNOS, IL-1β, TNF-α and COX-2 were elevated in NM and NH groups ($P<0.05$) (**B**a-d). Furthermore, the expressions of TNF-α, IL-1β, iNOS and COX-2 were validated by Western-blot analysis shown in (**C**a-b), and the expressions of iNOS, IL-1β, TNF-α and COX-2 in NH group were increased by 1.72-, 1.62-, 1.68- and 1.57-fold, respectively ($P<0.05$).

the testes. Taken together, the administration of La_2O_3 NPs may regulate testicular testosterone levels and expression of proteins involved in synthesis of testosterone (Figure 8).

Body weight was a key index evaluating the chemicals and drugs adverse effects.[26] During La_2O_3 NPs and MPs treatment period, the growth of body weight was no significant difference compared with the control group. La levels in the mouse testes significantly increased after the intragastric administration of La_2O_3 NPs in different doses and were considered the basis for the subsequent testes injury. Transmission electron microscopy results showed that La_2O_3 NPs could be transmitted and deposited in the testis and epididymis, causing vacuolation in the seminiferous epithelium in the NM and NH groups, and demonstrating that La_2O_3 NPs may change the testicular ultrastructure and cause reproduce toxicity.

NPs could cross the BTB and accumulate in the testis, resulting in decreased total sperm concentrations and sperm motility and increased number of abnormal sperm cells in the cauda epididymis.[27] Previous studies have

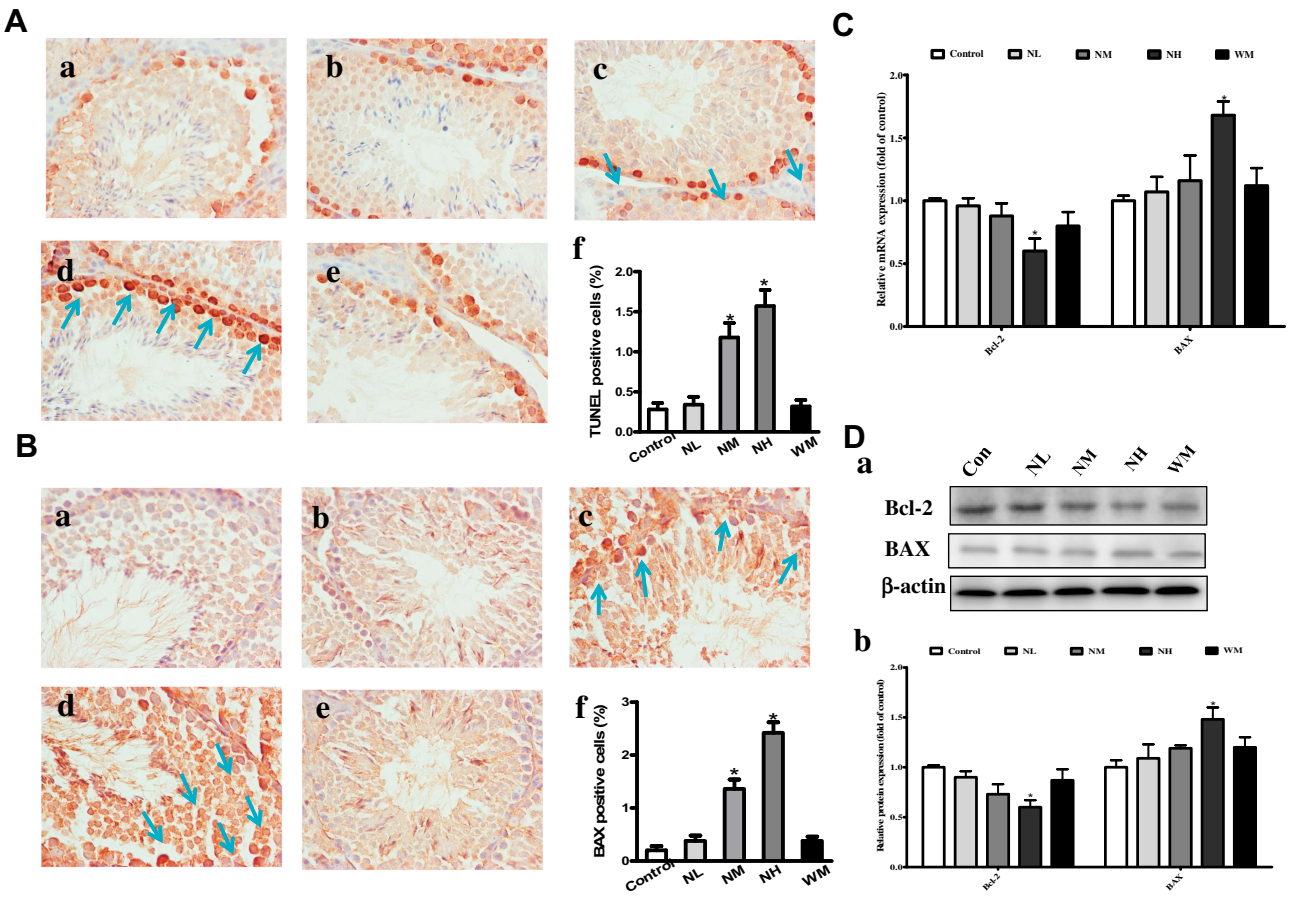

Figure 7 Effects of La_2O_3 NPs and MPs on testicular cells apoptosis. TUNEL and immunohistochemical staining of BAX (**A-B**) was detected at × 400 magnification. Apoptotic testicular cells in the control group (a), NL group (b), NM group (c), NH group (d) and WM group (e). Arrows indicated the positive cells, and histograms showing the percentages of TUNEL and BAX-positive cells (f). Exposure of mice to La_2O_3 NPs and MPs down-regulated of Bcl-2, and up-regulated both in the gene and protein levels of BAX in NH group compared with control group (Figure 7**C-D**) ($P<0.05$). The results of Bcl-2 and BAX protein expression in mouse testicular tissue were determined by Western blotting. β-Actin was used as the internal control (**D**a-b). *$P< 0.05$ vs control.

shown that using exposure protocols based on the daily administration of NPs have cytotoxic effects on testicular germ cells in a dose-dependent manner.[28] Other studies also showed that decreased sperm numbers and sperm concentrations were observed in male mice exposed to NPs.[29] In connection with these studies, we found that La_2O_3 NPs caused alteration in the structure of seminiferous epithelium and the production of sperm count, sperm motility, and the rate of sperm survival.

Recent studies suggested that nanoparticles pose risks to male reproductive health by altering sex hormone levels. Hormones played a key role in influencing the development of the reproductive system and subsequently in controlling its activities once developed.[30] LH stimulated testosterone production by LCs, whereas FSH stimulated the Sertoli cells to regulate spermatogenesis by secreting various factors that affect LCs function. Xiong et al found that the low production of sperm in the mice testis was associated with the suppression of GnRH expression that impaired testosterone synthesis.[31] Other studies demonstrated that low serum testosterone was frequently involved in some acute events in response to stress, exerting less suppression on the hypothalamus–pituitary connection. Consequently, high levels of LH occur, referred to as hypergonadotrophic hypogonadism.[32–34] Apart from causing direct damage to germ cells, La_2O_3 NPs were shown to negatively influence each level of the HPG axis, thereby impairing several hormones. La_2O_3 NPs decreased testosterone and GnRH serum levels and increased the level of LH. Steroidogenic acute regulatory protein was necessary for the transport of cholesterol into the mitochondria and was generally considered the rate-limiting factor in steroidogenesis.[35–37] Cholesterol side-chain enzyme CYP11A1 converted cholesterol into pregnenolone within the mitochondria, whereas CYP17A1 converted progesterone into androstenedione. It had been demonstrated that changes in the expression of CYP17A1 mRNA and protein may directly affect the level

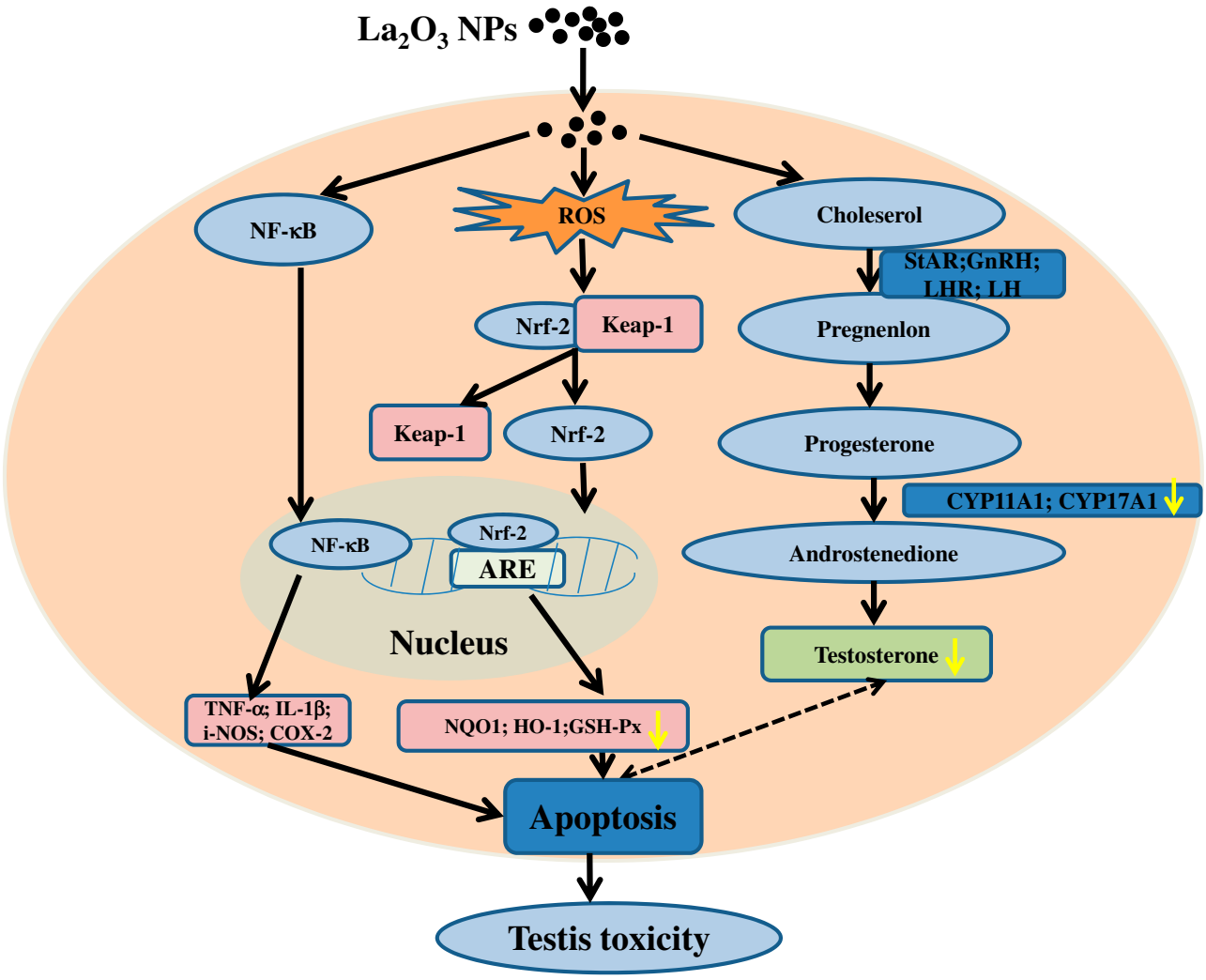

Figure 8 Schematic representation of possible mechanisms of La_2O_3 NPs contributing to the apoptosis of testes tissues.

of testosterone.[38,39] Our data suggested that La_2O_3 NPs may affect the HPG axis, resulting in hormonal imbalance, decreased expression of CYP11A1 and CYP17A1, and increased levels of LHR mRNA and protein.

Generally, oxidative stress has been considered to be an initiating event of reproductive toxicity. It occurs when the production of potentially destructive reactive oxygen species (ROS) exceeds the body's own natural antioxidant defenses. Therefore, MDA as a marker of lipid peroxidation, accumulates, while SOD as a major scavenger of ROS is depleted.[40] Excessive ROS modify and damage the lipids, eventually leading to mitochondrial malfunctions and apoptosis. Antioxidant enzyme CAT plays an important role in the elimination of ROS and provides the primary defense against oxidative stress.[41,42] Previous studies showed that in vivo exposure of mice to NPs could induce oxidative stress, resulting in decreased SOD activity and increased MDA level in the testis, further confirming that NPs could induce ROS and inflammasome activation, thus inducing oxidative stress in the testis and lead to apoptosis and necroptosis of the spermatogenic cells.[43–45] The present study showed that in vivo exposure of mice to La_2O_3 NPs could induce oxidative stress, leading to decreased SOD and CAT activities, and increased MDA levels in the testis, which was possibly caused by the toxic effects of oxidative stress and inflammatory mediators induced by La_2O_3 NPs.

Nrf-2 is a pivotal player in the cellular antioxidant defence system. As a master endogenous antioxidant defence, it plays an essential role in preventing oxidative disruption of the testes.[46,47] Nrf-2 regulates the expression of antioxidant proteins via interaction with the ARE. Under normal conditions, the cytoplasmic Nrf-2 mostly combines primarily binds with Keap-1 and is rapidly degraded by the ubiquitin-proteasome.[48] Nrf-2 accumulates in the nucleus in response to oxidative

stress and binds to the ARE. ARE is located in the promoter region of the genes that encode antioxidant phase II enzymes. These enzymes include HO-1, glutathione-S-transferase, NQO1 and other antioxidant enzymes and proteins, such as superoxide dismutase and GSH-Px.[49] Oxidative stress or stimulation of nucleophilic substances may trigger dissociation of Nrf-2 from Keap1, releasing free Nrf-2. It may also weaken the effect of the Keap-1-mediated protease on Nrf-2. Expression of downstream target genes plays an important role in maintaining redox homeostasis.[50] Long et al found that nuclear translocation of free Nrf-2 and binding with ARE trigger transcription of target genes downstream, including GSH-Px, HO-1 and NQO1.[51] The current results confirmed that mRNA and protein expression of NQO1, HO-1 and GSH-Px in the downstream region of the Nrf-2 signal pathway were all significantly decreased after 90 days intragastric administration of La_2O_3 NPs. Taken together, La_2O_3 NPs could inhibit the Nrf-2/ARE pathway and the expression of NQO1, HO-1 and GSH-Px. This inhibition resulted in oxidative stress and abrogation of the redox balance, thereby reducing the ability to resist La_2O_3 NP-induced oxidative stress in SCs, resulting in enhanced La_2O_3 NP-induced cell apoptosis.

Nuclear factor kappa light chain enhancer of activated B cells (NF-κB) has been considered the central regulator of the inflammatory process, which promotes the transcription of several pro-inflammatory mediators such as TNF-α, IL-1β, inducible nitric oxide synthase (iNOS), and cyclooxygenase-2 (COX-2). Additionally, NF-κB regulates testicular cell inflammation, and the activation of NF-κB affecting spermatogenesis and testicular functions has been significantly reported.[52,53] In addition, NF-κB plays a role in the regulation of testicular cells apoptosis, and it has been determined that the activation of NF-κB is proapoptotic in testicular cells.[54] This study found that NF-κB was activated in the testes by immunohistochemistry. Generally, cytokines stimulating the iNOS enzyme triggers the production of nitric oxide. Jin et al found that COX-2 is the major source of inflammation-associated prostaglandin synthesis that induces hypertrophy and loss of contractility in testicular peritubular cells, resulting in diminished sperm output.[55] Moreover, it has been widely observed that IL-1β stimulating iNOS and COX-2 levels can lead to inflammation.[56] It is reported that NPs can penetrate the cytomembrane and sediment in the mitochondria or even diffuse into the nucleus, subsequently resulting in cell death when its diameter is smaller than the size of the cellular organelles.[44] The present study indicated that La_2O_3 NPs caused spermatogenic cell apoptosis as detected by TUNEL assay, resulting in the occurrence of lesions in the testes and sperm cells. We also examined the activation of apoptotic pathways in the testes using BAX as the proapoptotic protein and Bcl-2 as the anti-apoptotic protein. Herein, BAX levels increased, while Bcl-2 levels decreased, confirming the enhanced apoptosis of testicular cells induced by La_2O_3 NPs.

Conclusion

Repeated exposure to high-dose (50 mg/kg BW) La_2O_3 NPs resulted in oxidative stress, inflammatory responses and apoptosis in testicle tissues. However, repeated low doses (5 mg/kg BW) of La_2O_3 NPs had no significant reproductive toxicity. Our results exhibited decreased nuclear translocation of Nrf-2, thus potentially leading to weaker induction of antioxidant defenses including a decrease in the activity of and the gene expression of NQO1, HO-1 and GSH-Px, and the transcription of Nrf-2-induced downstream target genes, suggesting that La_2O_3 NPs treatment inhibited the translocation of Nrf-2 from cytoplasm into the nucleus as well as the expression of downstream genes, thus abrogating Nrf-2-mediated defense mechanisms against oxidative stress.

Acknowledgments

This work was supported by National Natural Science Foundation of China (Nos. 81302323), The Natural Science Foundation of Hebei Province of China (C2019209478), Key Projects of Hebei Province (ZD2016007); and the PhD Research Startup Foundation of North China University of Science and Technology.

Disclosure

The authors declared they have no competing interests.

References

1. Espuche E, David L, Rochas C, et al. In situ generation of nanoparticulate lanthanum(III) oxide-polyimide films: characterization of nanoparticle formation and resulting polymer properties. *Polymer*. 2005;46(17):6657–6665. doi:10.1016/j.polymer.2005.05.020
2. Yue L, Ma C, Zhan X, White J, Xing B. Molecular mechanisms of maize seedling response to La2O3 NP exposure: water uptake, aquaporin gene expression and signal transduction. *Environ Sci Nano*. 2017;4(4):843–855. doi:10.1039/C6EN00487C
3. Gerber LC, Moser N, Luechinger NA, Stark WJ, Grass RN. Phosphate starvation as an antimicrobial strategy: the controllable toxicity of lanthanum oxide nanoparticles. *Chem Commun*. 2012;48(32):3869–3871. doi:10.1039/c2cc30903c
4. Brabu B, Haribabu S, Revathy M, et al. Biocompatibility studies on lanthanum oxide nanoparticles. *Toxicol Res (Camb)*. 2015;4(4):1037–1044. doi:10.1039/C4TX00198B
5. Guha A, Basu A. Role of rare earth oxide nanoparticles (CeO_2 and La_2O_3) in suppressing the photobleaching of fluorescent organic dyes. *J Fluoresc*. 2014;24(3):683–687. doi:10.1007/s10895-014-1375-2

6. Sisler JD, Pirela SV, Shaffer J, et al. Toxicological assessment of CoO and La_2O_3 metal oxide nanoparticles in human small airway epithelial cells. *Toxicol Sci*. 2016;150(2):418–428. doi:10.1093/toxsci/kfw005
7. Giovanni M, Tay CY, Setyawati MI, et al. Toxicity profiling of water contextual zinc oxide, silver, and titanium dioxide nanoparticles in human oral and gastrointestinal cell systems. *Environ Toxicol*. 2016;30(12):1459–1469. doi:10.1002/tox.22015
8. Priester JH, Yuan G, Mielke RE, et al. Soybean susceptibility to manufactured nanomaterials with evidence for food quality and soil fertility interruption. *Proc Natl Acad Sci*. 2012;109(37):14734–14735. doi:10.1073/pnas.1205431109
9. Balusamy B, Taştan BE, Ergen SF, Uyar T, Tekinay T. Toxicity of lanthanum oxide (La_2O_3) nanoparticles in aquatic environments. *Environ Sci Process Impacts*. 2015;17(7):1265–1270. doi:10.1039/C5EM00035A
10. Liu Y, Xu L, Dai Y. Phytotoxic effects of lanthanum oxide nanoparticles on maize (Zea mays L.). IOP conference series. *Earth Environ Sci*. 2018;113(1):013–020.
11. Ma Y, Zhang P, Zhang Z, et al. Origin of the different phytotoxicity and biotransformation of cerium and lanthanum oxide nanoparticles in cucumber. *Nanotoxicology*. 2015;9(2):9. doi:10.3109/17435390.2014.921344
12. Servin AD, White JC. Nanotechnology in agriculture: next steps for understanding engineered nanoparticle exposure and risk. *Nanoimpact*. 2016;1:9–12. doi:10.1016/j.impact.2015.12.002
13. Roberto DLTR, Alia S, Joseph H, et al. Terrestrial trophic transfer of bulk and nanoparticle La_2O_3 does not depend on particle size. *Environ Sci Technol*. 2015;49(19):11866–11874. doi:10.1021/acs.est.5b02583
14. Lim CH. Toxicity of two different sized lanthanum oxides in cultured cells and sprague-dawley rats. *Toxicol Res*. 2015;31(2):181–189. doi:10.5487/TR.2015.31.2.181
15. Shin SH, Lim CH, Kim YS, Lee YH, Kim SH, Kim JC. Twenty-eight-day repeated inhalation toxicity study of nano-sized lanthanum oxide in male sprague-dawley rats. *Environ Toxicol*. 2016;32(4):1226–40.
16. Sisler JD, Li R, Mckinney W, et al. Differential pulmonary effects of CoO and La_2O_3 metal oxide nanoparticle responses during aerosolized inhalation in mice. *Part Fibre Toxicol*. 2016;13(1):42. doi:10.1186/s12989-016-0155-3
17. Li R, Ji Z, C H C, et al. Surface interactions with compartmentalized cellular phosphates explain rare earth oxide nanoparticle hazard and provide opportunities for safer design. *ACS Nano*. 2014;8(2):1771–1783. doi:10.1021/nn406166n
18. Sun QC, Wu Y, Zhao F, Wang JJ. Maresin 1 ameliorates lung Ischemia/Reperfusion injury by suppressing oxidative stress via activation of the Nrf-2-Mediated HO-1 signaling pathway. *Oxid Med Cell Longev*. 2017;1–12.
19. Wang J, Li N, Zheng L, et al. P38-Nrf-2 signaling pathway of oxidative stress in mice caused by nanoparticulate TiO_2. *Biol Trace Elem Res*. 2011;140(2):186–197. doi:10.1007/s12011-010-8687-0
20. Bai D, Li Q, Xiong Y, et al. Editor's highlight: effects of intraperitoneal injection of SnS_2 flowers on mouse testicle. *Toxicol Sci*. 2017;161(2):388–400. doi:10.1093/toxsci/kfx220
21. Ahmmd SMA. Evaluating the effect of silver nanoparticles on testes of adult albino rats (Histological, immunohistochemical and biochemical study). *J Mol Histol*. 2016;48(1):1–19. doi:10.1007/s10735-016-9700-5
22. Boekelheide K, Shawna L, Kamin J. Role of Sertoli cells in injury-associated testicular germ cell apoptosis. *Exp Biol Med*. 2000;225(2):105–115. doi:10.1046/j.1525-1373.2000.22513.x
23. Yang H, Du L, Tian X, et al. Effects of nanoparticle size and gestational age on maternal biodistribution and toxicity of gold nanoparticles in pregnant mice. *Toxicol Lett*. 2014;230(1):10–18. doi:10.1016/j.toxlet.2014.07.030
24. Grassian VH, Adamcakova-Dodd A, Pettibone JM, O'Shaughnessy PI, Thorne PS. Inflammatory response of mice to manufactured titanium dioxide nanoparticles: comparison of size effects through different exposure routes. *Nanotoxicology*. 2007;1(3):211–226. doi:10.1080/17435390701694295
25. Lu X, Tian Y, Zhao Q, Jin T, Xiao S, Fan X. Integrated metabonomics analysis of the size-response relationship of silica nanoparticles-induced toxicity in mice. *Nanotechnology*. 2011;22(5):055101. doi:10.1088/0957-4484/22/5/055101
26. Khorsandi L, Orazizadeh M, Moradi-Gharibvand N, Hemadi M, Mansouri E. Beneficial effects of quercetin on titanium dioxide nanoparticles induced spermatogenesis defects in mice. *Environ Sci Pollut Res Int*. 2017;24(6):5595–5606. doi:10.1007/s11356-016-8325-2
27. Hong F, Zhao X, Si W, et al. Decreased spermatogenesis led to alterations of testis-specific gene expression in male mice following nano-TiO_2 exposure. *J Hazard Mater*. 2015;300:718–728. doi:10.1016/j.jhazmat.2015.08.010
28. Sundarraj K, Manickam V, Raghunath A, et al. Repeated exposure to iron oxide nanoparticles causes testicular toxicity in mice. *Environ Toxicol*. 2016;32(2):594–608. doi:10.1002/tox.22262
29. Hong F, Si W, Zhao X, et al. TiO_2 nanoparticles exposure decreases spermatogenesis via biochemical dysfunctions in the testis of male mice. *Agric Food Chemi*. 2015;63(31):7084–7092. doi:10.1021/acs.jafc.5b02652
30. Iavicoli I, Fontana L, Leso V, Bergamaschi A. The effects of nanomaterials as endocrine disruptors. *Int J Mol Sci*. 2013;14(8):16732–16801. doi:10.3390/ijms140816732
31. Xiong X, Zhong A, Xu H, Lobaccaro J-MA. Effect of cyanotoxins on the hypothalamic–pituitary–gonadal axis in male adult mouse. *PLoS One*. 2014;9(11):e106585–106594. doi:10.1371/journal.pone.0106585
32. Cheng Y-S, Dai D-Z, Dai Y. Testis dysfunction by isoproterenol is mediated by upregulating endothelin receptor A, leptin and protein kinase Cε and is attenuated by an endothelin receptor antagonist CPU0213. *Reprod Toxicol*. 2010;29(4):421–426. doi:10.1016/j.reprotox.2010.03.001
33. G L L, Yu F, D Z D, et al. Endoplasmic reticulum stress mediating downregulated StAR and 3-beta-HSD and low plasma testosterone caused by hypoxia is attenuated by CPU86017-RS and nifedipine. *J Biomed Sci*. 2012;19(1):4–15. doi:10.1186/1423-0127-19-4
34. Minutoli L, Micali A, Pisani A, et al. Flavocoxid protects against cadmium-induced disruption of the blood-testis barrier and improves testicular damage and germ cell impairment in mice. *Toxicol Sci*. 2015;148(1):311–329. doi:10.1093/toxsci/kfv185
35. Orazizadeh M, Khorsandi L, Absalan F, et al. Effect of beta-carotene on titanium oxide nanoparticles-induced testicular toxicity in mice. *J Assist Reprod Genet*. 2014;31(5):561–568. doi:10.1007/s10815-014-0184-5
36. Hasegawa T, Zhao L, K M C, et al. Developmental roles of the steroidogenic acute regulatory protein (StAR) as revealed by StAR knockout mice. *Mol Endocrinol*. 2000;14(9):1462–1471. doi:10.1210/mend.14.9.0515
37. Cao Z, Shao B, Xu F, et al. Protective effect of selenium on Aflatoxin B1-induced testicular toxicity in mice. *Biol Trace Elem Res*. 2017;180(2):233–238. doi:10.1007/s12011-017-0997-z
38. Weisser J, Landreh L, Söder O, et al. Steroidogenesis and steroidogenic gene expression in postnatal fetal rat Leydig cells. *Mol Cell Endocrinol*. 2011;341(1–2):18–24. doi:10.1016/j.mce.2011.03.008
39. Rosario B, Filippo M, Patrizia C, et al. Endurance exercise and conjugated linoleic acid (CLA) supplementation up-regulate CYP17A1 and stimulate testosterone biosynthesis. *PLoS One*. 2013;8(11):e79686–79696. doi:10.1371/journal.pone.0079686
40. Rukiye H, Sema U, Hacer H, et al. Protective effects of Ankaferd blood stopper on aspirin-induced oxidative mucosal damage in a rat model of gastric injury. *Toxicol Ind Health*. 2014;30(10):888–895. doi:10.1177/0748233712466134
41. Zhang H, Ji Z, Xia T, et al. Use of metal oxide nanoparticle band gap to develop a predictive paradigm for oxidative stress and acute pulmonary inflammation. *ACS Nano*. 2012;6(5):4349–4368. doi:10.1021/nn3010087

42. Suzanne Marie H, Ajay K, Sanjay S, et al. Bio-distribution and in vivo antioxidant effects of cerium oxide nanoparticles in mice. *Environ Toxicol*. 2013;28(2):107–118. doi:10.1002/tox.20704
43. Tsugita M, Morimoto N, Nakayama M. SiO_2 and TiO_2 nanoparticles synergistically trigger macrophage inflammatory responses. *Part Fibre Toxicol*. 2017;14(1):11. doi:10.1186/s12989-017-0192-6
44. Ren L, Zhang J, Zou Y, et al. Silica nanoparticles induce reversible damage of spermatogenic cells via RIPK1 signal pathways in C57 mice. *Int J Nanomedicine*. 2016;11:2251–2264. doi:10.2147/IJN.S102268
45. Jeong J, Song T, Chatterjee N, et al. Developing adverse outcome pathways on silver nanoparticle-induced reproductive toxicity via oxidative stress in the nematode Caenorhabditis elegans using a Bayesian network model. *Nanotoxicology*. 2019;12(10):1182–97.
46. Du D, Yao L, Zhang R, et al. Protective effects of flavonoids from, Coreopsis tinctoria, Nutt. on experimental acute pancreatitis via Nrf-2/ARE-mediated antioxidant pathways. *J Ethnopharmacol*. 2018;224:261–272. doi:10.1016/j.jep.2018.06.003
47. Yang SH, Yu LH, Li L, et al. Protective mechanism of sulforaphane on Cadmium-induced sertoli cell injury in mice testis via Nrf-2/ARE signaling pathway. *Molecules*. 2018;23(7):1774. doi:10.3390/molecules23071774
48. Yang SH, Long M, Yu LH, et al. Sulforaphane prevents testicular damage in kunming mice exposed to cadmium via activation of Nrf-2/ARE signaling pathways. *Int J Mol Sci*. 2016;17(10):1703. doi:10.3390/ijms17101703
49. Promsan S, Jaikumkao K, Pongchaidecha A, et al. Pinocembrin attenuates Gentamicin-induced nephrotoxicity in rats. *Physiol Pharmacol*. 2016;94(08):808–18.
50. Feng S, Xu ZF, Wang F, et al. Sulforaphane prevents methylmercury-induced oxidative damage and excitotoxicity through activation of the Nrf2-ARE pathway. *Mol Neurobiol*. 2017;54(1):375–391. doi:10.1007/s12035-015-9643-y
51. Long M, Yang SH, Shi W, et al. Protective effect of proanthocyanidin on mice Sertoli cell apoptosis induced by zearalenone via the Nrf-2/ARE signalling pathway. *Environ Sci Pollut Res*. 2017;24(1–4):1–10. doi:10.1007/s11356-017-0123-y
52. Hedger PM. Immunophysiology and pathology of inflammation in the testis and epididymis. *J Androl*. 2011;32(6):625–640. doi:10.2164/jandrol.111.012989
53. Reyes JG, Farias JG, Eva M, et al. The hypoxic testicle: physiology and pathophysiology. *Oxid Med Cell Longev*. 2012;2012(18):929285.
54. Guo Y, Sun J, Li T, et al. Melatonin ameliorates restraint stress-induced oxidative stress and apoptosis in testicular cells via NF-κB/iNOS and Nrf2/HO-1 signaling pathway. *Sci Rep*. 2017;7(1):9599. doi:10.1038/s41598-017-09943-2
55. Jin HK, Sun W, Dong WH, Moon HJ, Lee J. iNSC suppress macrophage-induced inflammation by repressing COX-2. *Vitro Cell Dev Biol Anim*. 2015;51(2):157–164. doi:10.1007/s11626-014-9816-4
56. Zhuang Z, Ye G, Huang B. Kaempferol alleviates the interleukin-1β-induced inflammation in rat osteoarthritis chondrocytes via suppression of NF-κB. *Int Med J Exp Clin Res*. 2017;23:3925–3931.